IEEE Photonics Journal
An IEEE Photonics Society Publication

Generation of Spiral Spin Density Vectors With A Circularly Polarized, Vortex Beam

Volume 12, Number 2, April 2020

Xiaoyan Pang
Wenhao Liu
Wenrui Miao

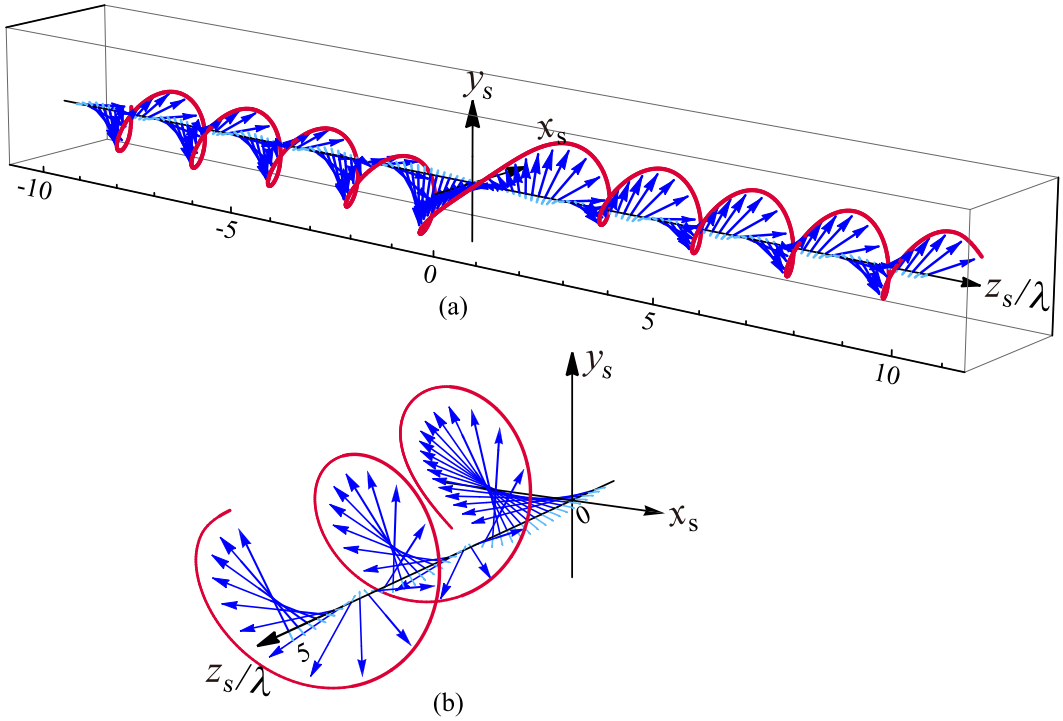

DOI: 10.1109/JPHOT.2019.2961148

Generation of Spiral Spin Density Vectors With A Circularly Polarized, Vortex Beam

Xiaoyan Pang, Wenhao Liu, and Wenrui Miao

School of Electronics and Information, Northwestern Polytechnical University, Xi'an 710072, China

DOI:10.1109/JPHOT.2019.2961148

Manuscript received October 9, 2019; revised November 28, 2019; accepted December 17, 2019. Date of publication December 20, 2019; date of current version April 3, 2020. This work was supported by the National Natural Science Foundations of China under Grants 11974281 and 11504296.
Corresponding author: Xiaoyan Pang (e-mail: xypang@nwpu.edu.cn).

Abstract: Spiral spin density vectors refer to the spiral trajectory of the spin density vectors in three dimensional (3D) space, and similar to the polarization Möbius strip, polarization knots and photonic wheel, are also special polarization structures in 3D optical field and only exist in three dimensions. In this article, we propose a new way to generate the spiral spin density vectors with a long spiral range. This is realized by strongly focusing a circularly polarized beam with one off-axis vortex. In this field, the spiral interval of spin density vectors theoretically always exists on the propagation axis, and its position can be controlled by the beam size parameter f/w_0. The polarization variation and the spiral spin density vectors are discussed analytically along the propagation direction. It is found that the spiral shape and spiral 'speed' can be adjusted by the off-axis distance of the vortex and the semi-aperture angle of the focusing system respectively. A special spiral behavior of the spin density vector at the geometrical focus is also observed in this focused field. The spiral spin density vectors supply a new rotational degree of freedom in 3D optical field and our finding may have applications in optical micro-manipulations.

Index Terms: Spin density vector, circular polarization, optical vortex, orbital angular momentum.

1. Introduction

Spiral structure is a basic structure of the world, which can be found from the double helix of DNA to a galaxy. The spiral is also a fundamental form in optics. The electric field vector of a circularly polarized field generates a spiral trajectory on propagation, while the wavefront of the electric field has a spiral shape in a vortex beam. Because of these two spiral behaviors, the optical beams can carry spin angular momentum (SAM) and orbital angular momentum (OAM), which is one of the fundamental theories in optics [1], [2]. SAM and OAM are important not only in fundamental research but also in many applications, for instance in laser cooling [3], microscopy [4], optical micro-manipulation [5] and wireless communications [6]. The interactions of SAM and OAM, or spin-orbit interactions (SOI) also play crucial roles in a variety of optical research [7]. As one result of the SOI in a strongly focused field, the spinning spin density vectors (also named SAM density vectors) compose a new spiral structure in a three-dimensional (3D) optical field [8]. This new spiral structure shows that not only the electric field vector can spin around its center but also the spinning plane of the electric field vector (i.e. the plane of the polarization ellipse) can spin around the optical axis on propagation. The spiral structure of spin density vectors supplies a new rotational degree of freedom in 3D optical fields, and like polarization Möbius strips [9]–[13],

topological polarization knots [14] and 'photonic wheel' [2], [15]–[18], is also a special polarization structure in three dimensions [19].

In a 3D optical field, such as a near field or a strongly focused field, the longitudinal component cannot be neglected any more, and it is not hard to demonstrate that the electric field can be polarized at any plane in 3D space. Since its orientation is always parallel (or anti-parallel) to the propagation direction, the spin density is usually treated as a scalar quantity in a two dimensional optical field [20]. However as the plane of polarization varies in three dimensions, the orientation of the spin density changes in 3D space, i.e., the spin density becomes 'spin density vector'. The fundamental research on polarization states and spin density vectors in a 3D optical field has been done in [21]–[26], including the 3D description of polarization, polarization singularities in three dimensions, and the 3D polarization algebra, etc. All the special polarization structures come from the fundamental properties of the 3D polarization. The 3D topological property and the special position of polarization singularity (the C point) cause the polarization Möbius strips and polarization knots respectively. The photonic wheel occurs when the spin density vector is perpendicular to the propagation direction, i.e. the SAM is transverse. While as a new polarization structure, the spiral structure of spin density vectors is formed as the spin density vectors rotates along a curve, which is first observed in a strongly focused, linearly polarized field [8]. However, in [8] there is a strict requirement for the numerical aperture (NA) to produce a relatively long spiral interval and two vortices should be used in incident field to generate the spiral spin density vectors. In this article we will show by focusing a circularly polarized beam, the spiral spin density vectors can be obtained with only one vortex embedded in the beam, and the spiral range is usually longer than that in [8]. Especially a special spiral behavior of the spin density vector will be observed in this focused field.

2. Theory

2.1 Polarization State in Three Dimensions

In three dimensions, a fully polarized electric field can be expressed by Jones vector as

$$\mathbf{E} = \begin{pmatrix} e_x \\ e_y \\ e_z \end{pmatrix} = \begin{pmatrix} |e_x| e^{i\phi_x} \\ |e_y| e^{i\phi_y} \\ |e_z| e^{i\phi_z} \end{pmatrix}. \tag{1}$$

It is easy to demonstrate that the polarization state in any point of a 3D fully polarized electric field is also a planar ellipse. There may be two common descriptions for the 3D polarization: one is the generalized Stokes parameters, and another is the spin density vector. The generalized Stokes parameters of the 3D fully polarized electric field are expressed as [25]

$$\left.\begin{aligned} &\Lambda_0 = |e_x|^2 + |e_y|^2 + |e_z|^2, \quad \Lambda_1 = 3|e_x||e_y|\cos\phi_{yx}, \\ &\Lambda_2 = 3|e_x||e_y|\sin\phi_{yx}, \quad \Lambda_3 = \frac{3}{2}(|e_x|^2 - |e_y|^2), \\ &\Lambda_4 = 3|e_x||e_z|\cos\phi_{zx}, \quad \Lambda_5 = 3|e_x||e_z|\sin\phi_{zx}, \\ &\Lambda_6 = 3|e_y||e_z|\cos\phi_{zy}, \quad \Lambda_7 = 3|e_y||e_z|\sin\phi_{zy}, \\ &\Lambda_8 = \frac{\sqrt{3}}{2}(|e_x|^2 + |e_y|^2 - 2|e_z|^2), \end{aligned}\right\} \tag{2}$$

where ϕ_{ij} is the phase difference between the two field components, i.e.,

$$\phi_{ij} = \phi_i - \phi_j. \quad (i, j = x, y, z) \tag{3}$$

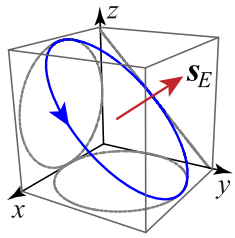

Fig. 1. Illustration of a polarization ellipse and its corresponding spin density vector in three dimensions. Here the blue curve indicates the polarization ellipse and the arrow shows its handedness. The spin density vector is illustrated by a red vector.

The spin density vector of electric field is another quantity to describe the 3D polarization state, which is defined as [2], [12], [23]

$$\mathbf{s}_E = \frac{\epsilon_0}{4\omega}\mathrm{Im}(\mathbf{E}^* \times \mathbf{E}), \tag{4}$$

with ϵ_0 the permittivity of free space and ω the angular frequency of the field. Im and * represent the imaginary part and the complex conjugate respectively. $\mathrm{Im}(\mathbf{E}^* \times \mathbf{E})$ is actually the normal vector of polarization ellipses [23], [24]. The shape of the polarization ellipse is reflected in the absolute value of the spin density vector, i.e., for a linear polarization the absolute value of the spin density vector is zero and for a circular polarization, it arrives at its maximum. Both the handedness and the orientation of the polarization ellipse define the direction of the spin density vector. An example of the polarization ellipse at a point and its spin density vector is shown in Fig. 1. The spin density vector can be expressed in terms of the generalized Stokes parameters, as

$$\mathbf{s}_E = \begin{pmatrix} s_E^{(x)} \\ s_E^{(y)} \\ s_E^{(z)} \end{pmatrix} = \frac{3\epsilon_0}{4\omega}\begin{pmatrix} |e_y||e_z|\sin\phi_{zy} \\ |e_x||e_z|\sin\phi_{zx} \\ |e_x||e_y|\sin\phi_{yx} \end{pmatrix} = \frac{\epsilon_0}{4\omega}\begin{pmatrix} \Lambda_7 \\ -\Lambda_5 \\ \Lambda_2 \end{pmatrix}. \tag{5}$$

One can easily find from Eq. (5) that when $|\mathbf{s}_E| = 0$, i.e., $|\Lambda_7| = |\Lambda_5| = |\Lambda_2| = 0$, the field is linearly polarized. It means that if $|e_i| \neq 0$, $(i = x, y, z)$, the polarization state is linear when $\phi_{ij} = N\pi$ $(i, j = x, y, z$; N is an integer). Also it has been proved that when $\Lambda_2^2 + \Lambda_5^2 + \Lambda_7^2 = 9\Lambda_0^2/4$, a pure circular polarization can be obtained [25], which indicates that the maximum value of the spin density $|\mathbf{s}_E|_{\mathrm{Max}}$ is

$$|\mathbf{s}_E|_{\mathrm{Max}} = \frac{3\epsilon_0}{8\omega}\Lambda_0 = \frac{3\epsilon_0}{8\omega}\left(|e_x|^2 + |e_y|^2 + |e_z|^2\right). \tag{6}$$

The spiral spin density vector describes the rotating behavior of the spin density vector around a certain curve. It is also a special structure in the 3D electric field. When we examine the spiral structure of the spin density vector, it is convenient to adopt the normalized spin density vector for analysis. The normalized spin density vector $\mathbf{s}_E^{nor}$ can be written as

$$\mathbf{s}_E^{nor} = \mathrm{Im}(\mathbf{E}^* \times \mathbf{E}) \Big/ \sqrt{\Lambda_2^2 + \Lambda_5^2 + \Lambda_7^2} = \begin{pmatrix} l \\ m \\ n \end{pmatrix} = \begin{pmatrix} \Lambda_7/\sqrt{\Lambda_2^2 + \Lambda_5^2 + \Lambda_7^2} \\ -\Lambda_5/\sqrt{\Lambda_2^2 + \Lambda_5^2 + \Lambda_7^2} \\ \Lambda_2/\sqrt{\Lambda_2^2 + \Lambda_5^2 + \Lambda_7^2} \end{pmatrix}, \tag{7}$$

where l, m, n represent the values of the normalized spin density vector at x, y, z directions respectively.

This spiral structure along a certain curve can be generated when the trace of the spin density vector in the normal plane of the curve is ellipses. For instance, if the spiral structure is composed along the z axis, the combination of the vectors l and m must form a circle with z in the x-y plane.

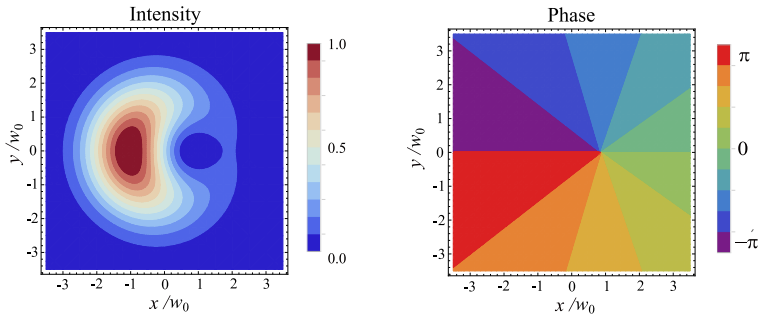

Fig. 2. Intensity and phase distribution of the incident beam at the waist plane. Here $q = -1$, $f = 1.2w_0$ and $a_0 = 0.43w_0$.

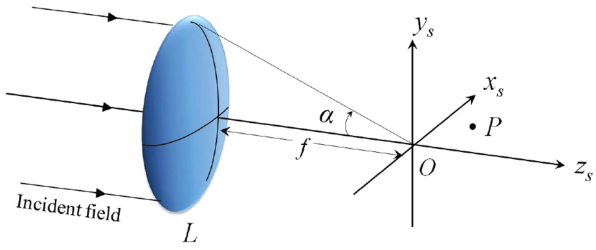

Fig. 3. Illustration of a high-numerical-aperture system.

2.2 Field Distribution in a Focal Region

In this section, we will discuss a new way to generate the spiral structure of the spin density vectors. Rather than a linearly polarized beam with two vortices adopted in [8], here we consider a (left-handed) circularly polarized Gaussian beam with one off-axis vortex located at ($r = a_0$, $\phi = 0^\circ$). At the waist plane this beam can be expressed as [27], [28]

$$E_0(r,\phi) = \begin{pmatrix} e_x^{(0)}(r,\phi) \\ e_y^{(0)}(r,\phi) \end{pmatrix} = e^{-r^2/w_0^2}(re^{iq\phi} - a_0)\begin{pmatrix} 1 \\ \mathrm{i} \end{pmatrix}, \tag{8}$$

where (r, ϕ) is the radial distance and the azimuthal angle respectively. w_0 is the waist radius, q is the topological charge of the vortex and the a_0 is its off-axis distance. The intensity and the phase distribution are illustrated in Fig. 2.

Then we choose $q = -1$ and suppose that this circularly polarized vortex beam is incident upon an aplanatic, high NA focusing system with focal length f and a semi-aperture angle α (see Fig. 3), and the waist plane of the beam is coincident with the entrance plane of this focusing system. According to the Richards-Wolf vectorial diffraction theory [29], the electric field in the focal region at an observation point $P(\rho_s, \phi_s, z_s)$ can be expressed as

$$\begin{aligned} E(\rho_s,\phi_s,z_s) = \begin{bmatrix} e_x \\ e_y \\ e_z \end{bmatrix} = -\frac{\mathrm{i}k}{2\pi}\int_0^{\alpha}\int_0^{2\pi} & f e^{-(f\sin\theta)^2/w_0^2}(f\sin\theta e^{-\mathrm{i}\phi} - a_0)\sqrt{\cos\theta}\sin\theta \\ \times & \begin{bmatrix} \cos\theta + \sin^2\phi(1-\cos\theta) + \mathrm{i}[(\cos\theta-1)\cos\phi\sin\phi] \\ (\cos\theta-1)\cos\phi\sin\phi + \mathrm{i}[\cos\theta + \cos^2\phi(1-\cos\theta)] \\ -\sin\theta\cos\phi + \mathrm{i}[-\sin\theta\sin\phi] \end{bmatrix} e^{\mathrm{i}k[z_s\cos\theta + \rho_s\sin\theta\cos(\phi-\phi_s)]}\mathrm{d}\phi\mathrm{d}\theta, \end{aligned} \tag{9}$$

where (ρ_s, z_s, ϕ_s) are the cylindrical coordinates in image space and k is the wave number ($k = 2\pi/\lambda$ and λ is the wavelength). The Abbe sine condition is also applied in Eq. (9), i.e., $r = f\sin\theta$. After integrating with respect to ϕ_s, we can get

$$e_x(\rho_s, \phi_s, z_s) = -\mathrm{i}k\int_0^{\alpha} P(\theta)(M_0^a + M_1^a + M_1^b + M_2^a + M_2^b)e^{\mathrm{i}kz_s\cos\theta}d\theta, \tag{10}$$

$$e_y(\rho_s, \phi_s, z_s) = -\mathrm{i}k\int_0^{\alpha} P(\theta)\mathrm{i}(M_0^a + M_1^a - M_1^b - M_2^a - M_2^b)e^{\mathrm{i}kz_s\cos\theta}d\theta, \tag{11}$$

$$e_z(\rho_s, \phi_s, z_s) = -\mathrm{i}k\int_0^{\alpha} P(\theta)(M_0^b + M_1^c + M_1^d)e^{\mathrm{i}kz_s\cos\theta}d\theta, \tag{12}$$

and

$$P(\theta) = fe^{-f^2\sin^2\theta/w_0^2}\sqrt{\cos\theta}\sin\theta, \tag{13}$$

$$M_0^a(\theta;\rho_s,\phi_s) = -\frac{1}{2}a_0(\cos\theta+1)J_0(k\rho_s\sin\theta), \tag{14}$$

$$M_0^b(\theta;\rho_s,\phi_s) = -f\sin^2\theta J_0(k\rho_s\sin\theta), \tag{15}$$

$$M_1^a(\theta;\rho_s,\phi_s) = \frac{1}{2}\,\mathrm{if}\sin\theta(\cos\theta+1)e^{-\mathrm{i}\phi_s}J_1(k\rho_s\sin\theta), \tag{16}$$

$$M_1^b(\theta;\rho_s,\phi_s) = \frac{1}{2}\,\mathrm{if}\sin\theta(\cos\theta-1)e^{\mathrm{i}\phi_s}J_1(k\rho_s\sin\theta), \tag{17}$$

$$M_1^c(\theta;\rho_s,\phi_s) = \mathrm{i}a_0\sin\theta\cos\phi_s J_1(k\rho_s\sin\theta), \tag{18}$$

$$M_1^d(\theta;\rho_s,\phi_s) = -a_0\sin\theta\sin\phi_s J_1(k\rho_s\sin\theta), \tag{19}$$

$$M_2^a(\theta;\rho_s,\phi_s) = \frac{1}{2}a_0(\cos\theta-1)\cos 2\phi_s J_2(k\rho_s\sin\theta), \tag{20}$$

$$M_2^b(\theta;\rho_s,\phi_s) = \frac{1}{2}\mathrm{i}a_0(\cos\theta-1)\sin 2\phi_s J_2(k\rho_s\sin\theta), \tag{21}$$

where J_i is the first kind Bessel function of order i. When $\rho_s = 0$, the axial field components can be obtained, as

$$e_x(z_s) = \mathrm{i}\frac{1}{2}a_0k\int_0^{\alpha}(\cos\theta+1)P(\theta)e^{\mathrm{i}kz_s\cos\theta}d\theta, \tag{22}$$

$$e_y(z_s) = -\frac{1}{2}a_0k\int_0^{\alpha}(\cos\theta+1)P(\theta)e^{\mathrm{i}kz_s\cos\theta}d\theta, \tag{23}$$

$$e_z(z_s) = \mathrm{i}kf\int_0^{\alpha}\sin^2\theta P(\theta)e^{\mathrm{i}kz_s\cos\theta}d\theta. \tag{24}$$

These field expressions show that there are three field components along the propagation axis, and as we will see in the following the phases of these three components change differently with propagation, which means that the polarization ellipses are also varied in 3D space along the axis. The relation between the e_x and e_y field components can be got easily, as $e_y = \mathrm{i}e_x$, which is similar to that in [8]. But we should note that the expressions for e_x, e_y and e_z components in this focused field are different from those in [8].

The Gouy phase, δ describes the phase difference between the actual (diffracted) field and a (non-diffracted) spherical wave converging to the focus in the half-space $z_s < 0$ and diverging from it in the other half-space $z_s > 0$ [see [30], Sec. 8.8.4]. For each field component on optical axis, a Gouy phase can be defined as

$$\delta_i(z_s) = \arg[e_i(z_s)] - kz_s. \quad (i = x, y, z) \tag{25}$$

From Eqs. (22)–(25), the following symmetry relations can be obtained

$$e_i^*(z_s) = -e_i(-z_s), \quad (i = x, z) \tag{26}$$

$$e_y^*(z_s) = e_y(-z_s), \tag{27}$$

which indicate

$$|e_i(z_s)| = |e_i(-z_s)|, \quad (i = x, z) \tag{28}$$

$$|e_y(z_s)| = |e_y(-z_s)|, \tag{29}$$

and

$$-\delta_i(z_s) = \pi + \delta_i(-z_s) \ (\text{mod } 2\pi), \quad (i = x, z) \tag{30}$$

$$-\delta_y(z_s) = \delta_y(-z_s) \ (\text{mod } 2\pi), \tag{31}$$

thus at the geometrical focus

$$\delta_i(0) = \pm\pi/2 \ (\text{mod } 2\pi), \quad (i = x, z) \tag{32}$$

$$\delta_y(0) = \pi \ (\text{mod } 2\pi). \tag{33}$$

3. Result

3.1 Polarization Changes in Three Dimensions

In this part the polarization states along the optical axis will be discussed. From the definition of the Gouy phase Eq. (25), one can find that in a strongly focused field, the phase difference between two field components ϕ_{ij} is actually the Gouy phase difference δ_{ij}, i.e.,

$$\delta_{ij} = \delta_i - \delta_j = \phi_{ij}, \quad (i, j = x, y, z) \tag{34}$$

Therefore, the points along the optical axis have the following relations:

$$|e_x| = |e_y|, \tag{35}$$

$$\phi_{yx} = \delta_{yx} = \pi/2, \tag{36}$$

$$\phi_{zy} = \delta_{zy} = \delta_{zx} - \pi/2. \tag{37}$$

By substituting Eqs. (35)–(37) into the expressions of the Stokes parameters Eq. (2), we can get

$$\Lambda_2 = 3|e_x|^2, \tag{38}$$

$$\Lambda_5 = 3|e_x||e_z| \sin\delta_{zx}, \tag{39}$$

$$\Lambda_7 = -3|e_x||e_z| \cos\delta_{zx}, \tag{40}$$

from which one can obtain that on axis $|\Lambda_2|^2 + |\Lambda_5|^2 + |\Lambda_7|^2 = 9|e_x|^4 + 9|e_x|^2|e_z|^2$ is smaller than $9|\Lambda_0|^2/4 = 9|e_x|^4 + 9|e_x|^2|e_z|^2 + 9|e_z|^4/4$ (if $|e_z| \neq 0$), which means that it is hard to find a point with circular polarization on axis. Eqs. (22)–(24) show in almost all the cases $|e_x| \neq 0$ and $|e_z| \neq 0$. Based on the analysis in previous section, here $\delta_{yx} = \pi/2 \neq N\pi$ (N is an integer) indicates that the electric field along the optical axis is also hardly linearly polarized (except the points with $|e_x| = 0$). Therefore generally the polarization states along the optical axis are typically elliptical (not linear or circular). The polarization ellipses are shown at selected points in Fig. 4, where the 3D polarization ellipses are illustrated by blue curves. Here the ellipses in gray are projections of the 3D polarization ellipse in x_s-y_s, x_s-z_s and y_s-z_s planes.

First the polarization ellipses in Fig. 4 changes dramatically along the propagation axis and the orientation of the polarization planes can be in different directions. Second, the projections of the polarization ellipses on the x_s-y_s plane are always circular [due to Eqs. (35) and (36)]. Third, the polarizations are linear in x_s-z_s plane or in y_s-z_s plane when the Gouy phase difference δ_{zx} is $N\pi$ or $(2N+1)\pi/2$ (N is an integer), which can be observed at points $z_s = 0$, ± 1.63, ± 3.58,

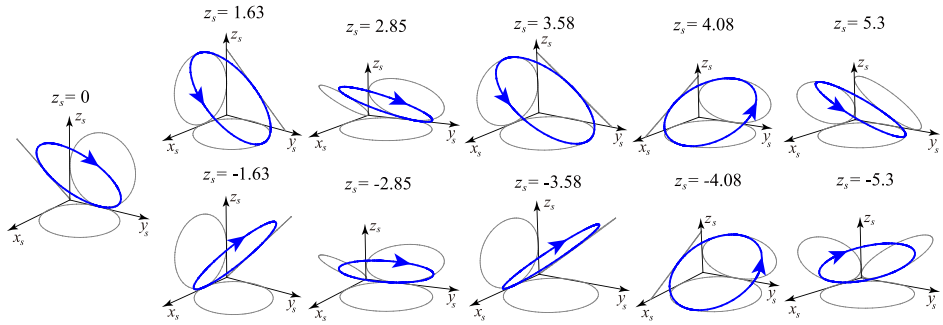

Fig. 4. Polarization ellipses in 3D at selected points on z_s axis (with unit λ). Here $\alpha = 60^\circ$, $f = 1.2w_0$ and $a_0 = 0.43w_0$.

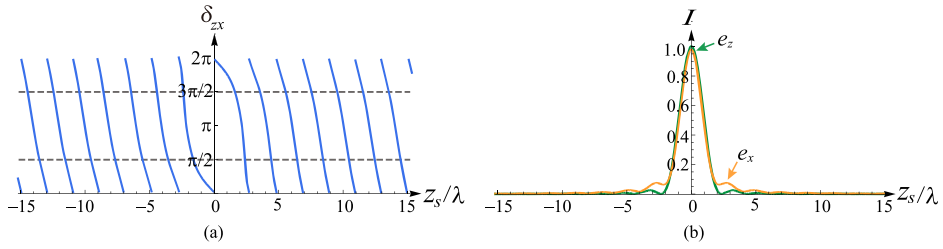

Fig. 5. The Gouy phase difference between the e_x and e_z components (a), and the intensity of these two components along the optical axis (b). Here $\alpha = 60^\circ$, $f = 1.2w_0$ and $a_0 = 0.43w_0$.

± 4.08. The Gouy phase difference δ_{zx} is shown in Fig. 5(a), where two dashed lines denote the values $\pi/2$ and $3\pi/2$ of δ_{zx}. Especially, at points $z_s = \pm 1.63$, δ_{zx} is $3\pi/2$ or $\pi/2$ ($\delta_{zy} = 0$), and through adjusting a_0 (in this case a_0 is chosen as $0.43\omega_0$), the amplitude ratio can satisfy $|e_x/e_z| = 1$ [see Fig. 5(b)]. The polarization ellipses hence at points $z_s = \pm 1.63$ are pure circular in x_s-z_s plane, while they are linear in y_s-z_s plane and circular in x_s-y_s plane. Note that the Gouy phase is independent of the parameter a_0 (except the case of $a_0 = 0$).

3.2 Spiral Spin Density Vectors Along the Optical Axis

Applying Eqs. (35)–(37) into Eq. (7), the normalized spin density vector at x_s, y_s and z_s directions becomes:

$$l = -\cos\delta_{zx}/\sqrt{|e_x/e_z|^2 + 1}, \tag{41}$$

$$m = -\sin\delta_{zx}/\sqrt{|e_x/e_z|^2 + 1}, \tag{42}$$

$$n = 1/\sqrt{|e_z/e_x|^2 + 1}. \tag{43}$$

These equations show that the orientation of the spin density vector is dependent on two factors: the intensity ratio $|e_x/e_z|$ and the Gouy phase difference δ_{zx}, which is consistent with that in [8]. Note that although the Eqs. (41–43) seem same to Eqs. (14)–(15) in [8], the orientation of the spin density vectors here is quite distinct from that in [8] because the different expressions of the $|e_x/e_z|$ and δ_{zx} in both two fields. From the symmetry relations of e_i and δ_{ij} (i, $j = x, y, z$), Eqs. (28)–(31), we can find the symmetry relations for l, m and n, as

$$l(z_s) = l(-z_s), \tag{44}$$

$$m(z_s) = -m(-z_s), \tag{45}$$

$$n(z_s) = n(-z_s), \tag{46}$$

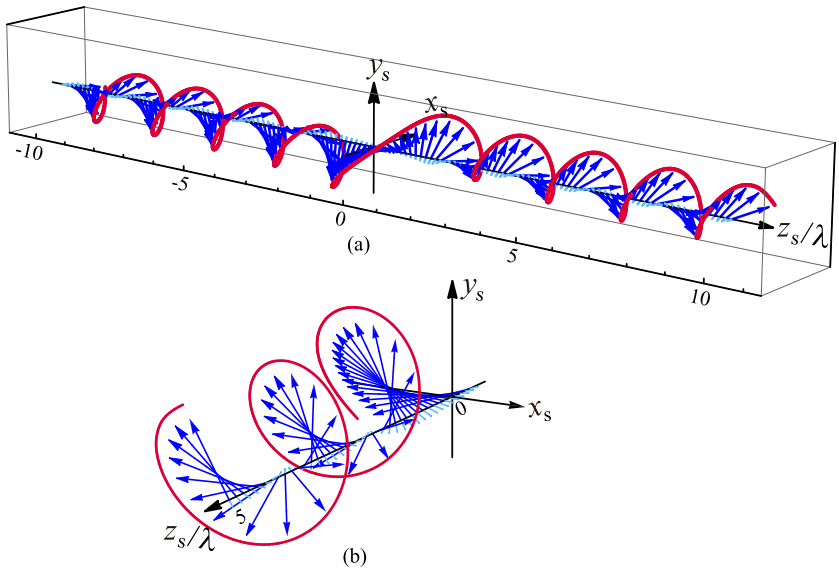

Fig. 6. Spin density vectors along the optical axis. (b) is a section of (a) but is seen from another perspective. Here $\alpha = 60^\circ$, $f = 1.2w_0$ and $a_0 = 0.43w_0$.

which can be observed in Fig. 4 where the orientations of the polarization ellipses at two symmetric points are opposite at y_s direction. The normalized spin density vectors are drawn in Fig. 6 with the same parameters of Figs. 4 and 5. The blue arrow denote the spin density vectors and the red curve is the envelope of these vectors. [Note that for clarity, the plot range in Fig. 6(a) is chosen as $(-10\lambda, 10\lambda)$, but actually the spiral range is not limited to this range.]

It is clearly to see that the spin density vector is rotating around the z_s axis on propagation, i.e., the spiral behavior of the spin density vectors is observed, which also means that the planes of polarization ellipses of the axial points are also rotating in three dimensions with propagation. If it is seen from the positive z_s axis, the handedness of this spiral is clockwise in the x_s-y_s plane. Here we will show that this spiral structure is caused by the Gouy phase.

As it is analyzed is Sec. 2.2, when the spiral behavior of the spin density vectors is generated along the z_s axis, the trajectory of the vector $l\hat{x}_s + m\hat{y}_s$ will form circles in the x_s-y_s plane with the value of z_s. If $|e_x| \neq 0$ and $|e_z| \neq 0$, from Eqs. (41) and (42) we can simply treat $l' = -\cos\delta_{zx}$ and $m' = -\sin\delta_{zx}$ as the spin density vectors at the x_s and the y_s directions respectively. l' and m' also can be written as $l' = -\mathrm{Re}[e^{\mathrm{i}\delta_{zx}}]$ and $m' = -\mathrm{Re}[e^{\mathrm{i}(\delta_{zx}-\pi/2)}]$. Thus it is easy to find that if δ_{zx} is a monotonic function of z_s on an interval, the spin density vector will rotate in the x_s-y_s plane with z_s on that interval.

Fig. 5(a) shows that the Gouy phase difference δ_{zx} is actually monotonically decreased from $z_s = -15\lambda$ to 15λ, if the δ_{zx} is not only confined in one period $(0 - 2\pi)$. Therefore the spin density vector rotates clockwise in the x_s-y_s plane along the z_s axis. Note that in [8] the Gouy phase difference is monotonically increasing function of z_s and thus the handedness of the spiral spin density vectors there is counterclockwise.

This monotonic property of the Gouy phase difference δ_{zx} is a result of the spin-orbital interaction (SOI) in a high NA system. Let's look at the incident field first. The amplitude of the incident field, Eq. (8) can be written as a superposition of two beams, one is a Gaussian vortex beam $e^{-r^2/w_0^2}re^{-\mathrm{i}\phi}$, and another is a fundamental Gaussian beam $-a_0e^{-r^2/w_0^2}$. Second because of the SOI, in a high NA system that the left circularly polarized, Gaussian vortex beam with charge -1 will generate an e_z component along the propagation axis, while the left circularly polarized, fundamental Gaussian beam will have a circularly polarized component ($e_y = \mathrm{i}e_x$). The wavefront spacings or the effective wavelengths for these two field components are quite different, and the Gouy phase of the e_z usually

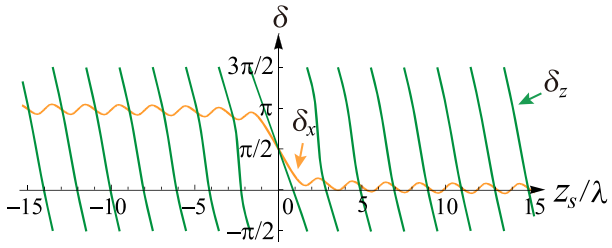

Fig. 7. Gouy phases of the e_x and e_z components along the z_s axis. Here $\alpha = 60^\circ$, $f = 1.2w_0$ and $a_0 = 0.43w_0$.

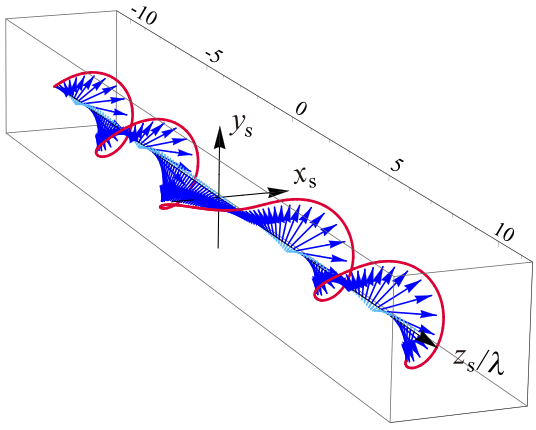

Fig. 8. Spin density vectors along the optical axis. Here $\alpha = 40^\circ$, $f = 1.2w_0$ and $a_0 = 0.43w_0$.

changes faster than that of the circularly polarized component [31] (note: the circularly polarized component, the e_x component and e_y component have the same Gouy phase except for a $\pi/2$ difference). The absolute value of the slope of the δ_z in most regions on the z_s axis is bigger than that of the δ_x (see Fig. 7, where the Gouy phases of the e_x and e_z components are illustrated), thus a monotonic interval for the δ_{zx} is formed and the spiral structure of the spin density vector is observed. It is also worth stating that if the polarization of the incident field is right circular or the topological charge is $+1$ (or other values), the spiral spin density vectors will disappear, furthermore if the initial polarization is changed, the number of the vortices at least needs raising to 2 to generate this special structure. Therefore we can say that the method presented in this article is simplest one in strongly focusing systems for generating the spiral structure of spin density vectors.

The spiral behavior of the spin density vectors in this focused field also can be adjusted by the semi-aperture angle α and the off-axis distance a_0, which is also analyzed in [8]. When the semi-aperture angular α is increased, the spin density vectors generally rotate more circles in the same monotonic interval, which is caused by the increase of the Gouy phase difference [31]. The spin density vectors with α decreased to 40° is drawn in Fig. 8. Comparing Fig. 8 with Fig. 6(a), we can see that when the semi-aperture angle α is decreased, the spin density vectors will rotate 'slower' (less circles). This also can seen in a 2D parametric plot of $z_s * l' (= -z_s \mathrm{Re}[e^{i\delta_{zx}}])$ and $z_s * m' (= -z_s \mathrm{Re}[e^{i(\delta_{zx} - \pi/2)}])$, with the variable z_s as the parameter, which is presented in Fig. 9. It is clear to see that the spin density vectors rotate 4 circles and a half for $\alpha = 60^\circ$, while they only rotate less than 2 circles for $\alpha = 40^\circ$ in the same interval with z_s from 0 to 10λ.

Eqs. (22)–(24) show that the a_0 does not have a contribution to the Gouy phases, which also means that a_0 does not affect on the rotational behavior of the spin density vectors, but it can change the shape of the spiral trajectory. When the off-axis distance a_0 becomes bigger, from Eqs. (22)–(24) we can see that the $|e_z/e_x|$ becomes smaller, hence the z_s component of the spin

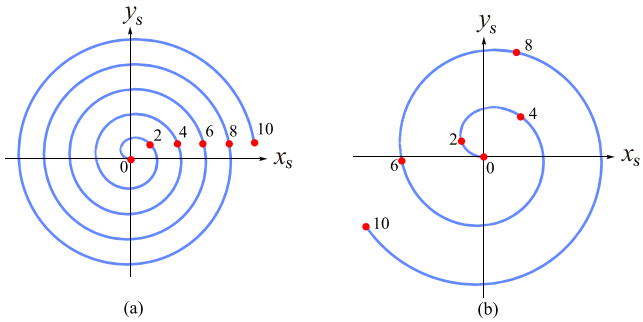

Fig. 9. Parametric plot of ($z_s * l'$, $z_s * m'$) along the optical axis z_s. The dots correspond with the values $z_s/\lambda = 0, 2, ..., 10$. The semi-aperture angle α was taken to be 60° (a) and 40° (b). Here $f = 1.2w_0$ and $a_0 = 0.43w_0$.

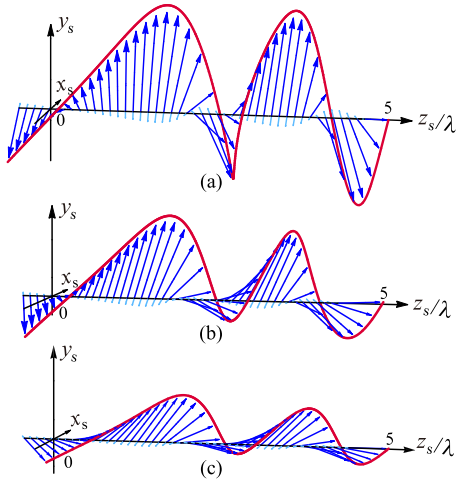

Fig. 10. Spin density vectors along the optical axis for different values of a_0. (a) $a_0 = 0.10w_0$, (b) $a_0 = 0.43w_0$, (c) $a_0 = 1.00w_0$. Here $\alpha = 60°$, $f = 1.2w_0$.

density vector, n, is increased. This can be seen in Fig. 10, where a_0 is increased from $0.10w_0$, $0.43w_0$ to $1.00w_0$, while the shape of the spiral becomes more and more parallel to the z_s axis.

The advantage of present structured field over that in [8] is that we can always find a relatively long monotonic interval on the optical axis, even the semi-aperture angular α is small. It was shown in [8] that as the semi-aperture angle α was decreased, the monotonic interval became shorter, for example when α was decreased to 45°, the monotonic interval shrank to a distance around -7λ to 7λ. However, it is not the case in current focused field. In Fig. 11, the Gouy phase difference δ_{zx} along the optical axis in current field is presented for both $\alpha = 45°$ and 30°. Here only the value on the positive part of the z_s is illustrated and the negative part can be got easily from the symmetry relations Eqs. (30) and (34). We can see that the monotonic interval does not get shorter when α is decreased. It means that a spiral structure of the spin density vectors can be obtained in this focused field without a strict requirement for the NA.

Although the monotonic interval does not shrink by decreasing the semi-aperture angle α, the spiral range of the spin density vectors can be adjusted by the the beam size parameter of the incident beam f/w_0. It is shown in Figs. 12(a) and 12(a') of that when f/w_0 is increased to 1.5, the spin density vectors vibrate at the distance close to the focus and start to rotate nearly after $z_s = 4\lambda$, i.e., the spiral range is broken from the geometric focus. As f/w_0 is increased to 1.8 [see Figs. 12(b) and 12(b')], the non-spiral range spreads to $0 \sim 8\lambda$. It is worth noting that from the

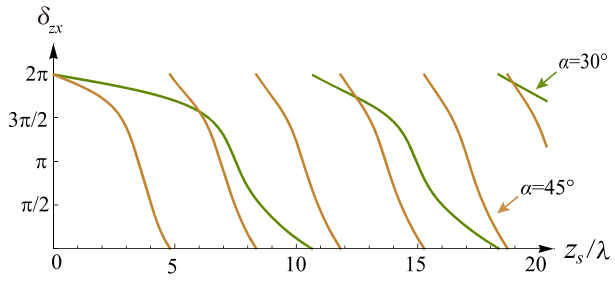

Fig. 11. The Gouy phase difference δ_{xz} along the optical axis for different values of α. Here $f = 1.2w_0$ and $a_0 = 0.43w_0$

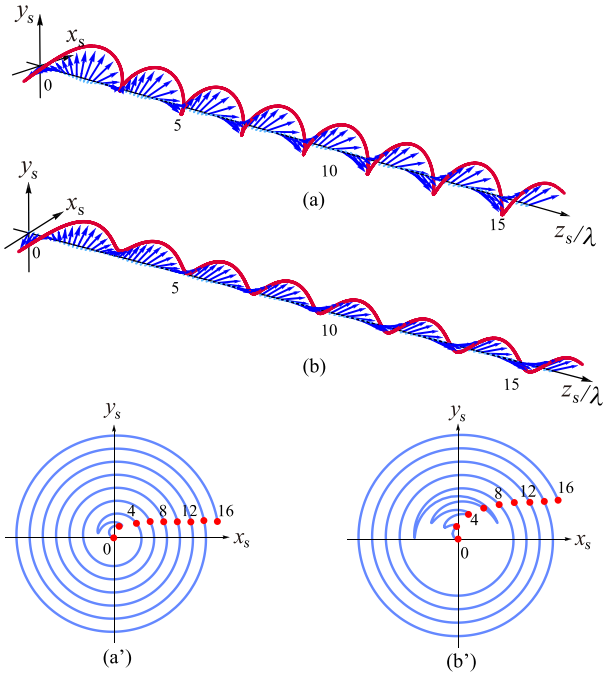

Fig. 12. Spin density vectors along the optical axis with (a) $f = 1.5w_0$ and (b) $f = 1.8w_0$, and the corresponding parametric plots of ($z_s * l'$, $z_s * m'$) with (a') $f = 1.5w_0$ and (b') $f = 1.8w_0$. The red dots denote the values at $z_s/\lambda = 0, 2, ..., 16$. Here $\alpha = 60^\circ$ and $a_0 = 0.43w_0$.

symmetry relations Eqs. (44)–(46), the non-spiral range on the whole z_s axis is double that on the positive z_s axis. This result shows that as the beam size parameter f/w_0 increases to a certain value, the non-spiral structure of the spin density vectors can appear from the focus, and the non-spiral range will increase with f/w_0. This phenomenon can be explained as a result of the effect of the field distribution at the entrance plane on the Gouy phases. In a focusing system, usually the focal length f is fixed, thus increasing f/w_0 means decreasing the beam radius of the incident field w_0. When w_0 is decreased, the contribution from the rays with big diffraction angles on the axial wavefront spacings is reduced, which causes the Gouy phase difference between the circular polarized component and the longitudinal polarized component becomes irregular near the focus [31], [32], i.e., δ_{zx} will not be monotonically decreased or increased there. Thus the vibrating behavior, or the non-spiral behavior of the spin density vectors appears. (Note that the critical value of f/w_0 for appearing the non-spiral structure is dependent on the semi-aperture angle α.)

It is also very interesting to see another 'special spiral spin density vectors' at the focus. When we observe Eqs. (22), (24), (32) and (34), we can find that at the geometrical focus, δ_{zx} is not

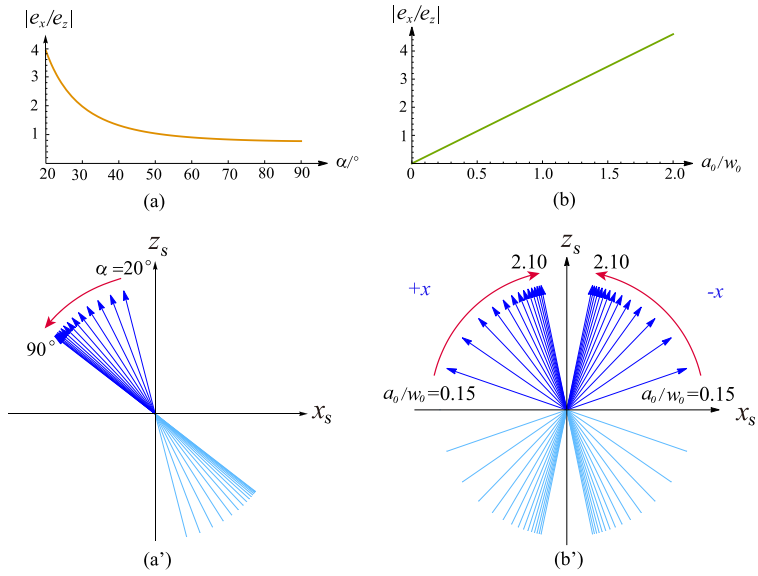

Fig. 13. Rotation of the spin density vector at focus. The variation of $|e_x/e_z|$ with semi-aperture angle α (a), the off-axis distance a_0 (b). The rotation of the spin density vector with α (a'), a_0 (b'). $+x$ and $-x$ denote the focused fields with the vortex located at $+x$ axis and $-x$ axis (in the entrance plane) respectively. In all plots, when the parameters are not variables, they are chosen as $\alpha = 60^\circ$, $a_0 = 0.43w_0$ and $f = 1.2w_0$.

influenced by the semi-aperture angle α or the off-axis distance a_0. $\delta_{zx}(\rho_s = 0, \phi_s = 0)$ is always equal to 0 or π (here 0 and π correspond to the focused field with the off-axis vortex located at the $+x$ axis and the $-x$ axis respectively). So at the focus, Eqs. (41)–(43) become $l = \mp/\sqrt{|e_x/e_z|^2 + 1}$, $m = 0$, $n = 1/\sqrt{|e_z/e_x|^2 + 1}$ (here $-$ and $+$ in the expression of l correspond to $\delta_{zx} = 0$ and $\delta_{zx} = \pi$ respectively). These expressions mean that first the spin density vector at the focus always lies in the x_s-z_s plane and $l^2 + n^2 = 1$. Second, l and n are both monotonic functions of $|e_x/e_z|$. Eqs. (22) and (24) show that $|e_x/e_z|$ is also a monotonic function of α or a_0. Therefore the spin density vector at the focus can rotate in the x_s-z_s plane with the semi-aperture angle α or the off-axis distance a_0. This type of rotation is independent of the Gouy phase. The relations between $|e_x/e_z|$ and α, $|e_x/e_z|$ and a_0 are illustrated in Figs. 13(a) and 13(b). Figs. 13(a') and 13(b') show the rotation behaviors of the spin density vector at the focus with the variations of α and a_0 respectively. In Fig. 13(a') α is selected from 20° to 90° with an interval 5°. In Fig. 13(b') a_0 changes from $0.15w_0$, $0.30w_0$, $0.45w_0$, ..., to $2.10w_0$. In order to make the result more general, in Fig. 13(b') the spin density vectors of the focused field with the off-axis vortex located at the negative part of the x axis of the incident field are also shown.

From Fig. 13, as well as Eqs. (22) and (24), we can obtain the following conclusions. First, as α increases or a_0 decreases, the spin density vector will rotate from near the z_s to near the x_s axis, and it never reach the z_s axis or the x_s. Second, when α or a_0 gets bigger, the rotation of the spin density vector slows down. Third, strictly speaking, the range of the rotation in this type is always within a quarter. Although when the vortex in the entrance plane moves along the x axis from the positive part to the negative part, the spin density vectors can span two quarters, the rotation is actually not continues (i.e. the rotation is still in one quarter). This discontinuity happens because when $a_0 = 0$, the polarization is linear at the focus (i.e., a 'L-point'), and according to the rule of topological reactions for polarization singularities, the polarizations will have opposite handedness at the two sides of a L-point, i.e., the direction of the spin density vector will change 180° as the vortex passes through the focus. In addition, the specific range of the rotation at the focus depends on both the semi-aperture angle α and the off-axis distance a_0.

4. Conclusions

In this article, we supply a simple way to generate the spiral spin density vectors in a 3D optical field. It is achieved by focusing a circularly polarized beam with an off-axis vortex in a high NA system. Comparing with the method in [8], the current way uses fewer vortices and produces a longer spiral range for the spin density vectors. The properties of the spiral spin density vectors on the optical axis, as well as the variations of the polarization in three dimensions, are analyzed. Our result shows that this spiral spin density vectors is mainly caused by the Gouy phase difference which is also a result of SOI in a strongly focusing system. The shape of the spiral structure of the spin density vectors can be adjusted by the off-axis distance a_0, while the rotation of the spin density vectors can speed up by increasing the semi-aperture angle α. Although there always exist the intervals for the spiral spin density vectors in this focused field, the beam size parameter f/w_0 can be used to control the spiral range of the spin density vectors. By increasing f/w_0, the spiral range can break from the focus and the non-spiral range will spread from the focus with the increase of f/w_0. It is also found that at the focus the spin density vector will rotate with α or a_0. This rotation behavior is independent of the Gouy phase, which can be treated as a 'special spiral spin density vector'. The spiral spin density vectors not only supply a completely new rotational degree of freedom in optical manipulations, but also support a new structure of 3D optical fields. Our finding may get applied in optical trapping and have implications in studying the unique optical structures in three dimensions.

References

[1] L. Allen, S. M. Barnett, and M. J. Padgett, *Optical Angular Momentum*. Bristol, U.K.: IoP, 2003.
[2] K. Y. Bliokh, A. Y. Bekshaev, and F. Nori, "Extraordinary momentum and spin in evanescent waves," *Nat. Commun.*, vol. 5, no. 3, 2014, Art. no. 3300.
[3] S. Stenholm, "The semiclassical theory of laser cooling," *Rev. Modern Phys.*, vol. 58, no. 3, pp. 699–739, 1986.
[4] E. Rittweger, K. Y. Han, S. E. Irvine, C. Eggeling, and S. W. Hell, "STED microscopy reveals crystal colour centres with nanometric resolution," *Nature Photon.*, vol. 3, no. 3, pp. 144–147, 2009.
[5] K. Dholakia and T. Čižmár, "Shaping the future of manipulation," *Nature Photon.*, vol. 5, no. 6, pp. 335–342, 2011.
[6] J. Wang *et al.*, "Terabit free-space data transmission employing orbital angular momentum multiplexing," *Nature Photon.*, vol. 6, pp. 488–496, 2012.
[7] K. Y. Bliokh, F. J. Rodríguez-Fortuño, F. Nori, and A. V. Zayats, "Spin-orbit interactions of light," *Nature Photon.*, vol. 9, no. 12, pp. 156–163, 2015.
[8] X. Pang and W. Miao, "Spinning spin density vectors along the propagation direction," *Opt. Lett.*, vol. 43, no. 19, pp. 4831–4834, Oct 2018. [Online]. Available: http://ol.osa.org/abstract.cfm?URI=ol-43-19-4831
[9] I. Freund, "Cones, spirals, and möbius strips, in elliptically polarized light," *Opt. Commun.*, vol. 249, no. 1–3, pp. 7–22, 2005.
[10] I. Freund, "Optical möbius strips and twisted ribbon cloaks," *Opt. Lett.*, vol. 39, no. 4, pp. 727–730, 2014.
[11] T. Bauer *et al.*, "Observation of optical polarization möbius strips," *Science*, vol. 347, no. 6225, pp. 964–966, 2015.
[12] T. Bauer, M. Neugebauer, G. Leuchs, and P. Banzer, "Optical polarization möbius strips and points of purely transverse spin density," *Phys. Rev. Lett.*, vol. 117, no. 1, 2016, Art. no. 013601.
[13] K. Y. Bliokh, M. A. Alonso, and M. R. Dennis, "Geometric phases in 2D and 3D polarized fields: Geometrical, dynamical, and topological aspects," *Rep. Prog. Phys.*, vol. 82, no. 12, 2019, Art. no. 122401.
[14] H. Larocque *et al.*, "Reconstructing the topology of optical polarization knots," *Nature Phys.*, vol. 14, no. 11, pp. 1079–1082, 2018.
[15] T. Bauer, S. Orlov, U. Peschel, P. Banzer, and G. Leuchs, "Nanointerferometric amplitude and phase reconstruction of tightly focused vector beams," *Nature Photon.*, vol. 8, no. 1, pp. 23–27, 2014.
[16] M. Neugebauer, T. Bauer, A. Aiello, and P. Banzer, "Measuring the transverse spin density of light," *Phys. Rev. Lett.*, vol. 114, no. 6, 2015, Art. no. 063901.
[17] A. Aiello, P. Banzer, M. Neugebauer, and G. Leuchs, "From transverse angular momentum to photonic wheels," *Nature Photon.*, vol. 9, no. 12, pp. 789–795, 2015.
[18] K. Y. Bliokh and F. Nori, "Transverse and longitudinal angular momenta of light," *Phys. Rep.*, vol. 592, pp. 1–38, 2015.
[19] H. Rubinsztein-Dunlop *et al.*, "Roadmap on structured light," *J. Opt.*, vol. 19, no. 1, 2016, Art. no. 013001.
[20] A. Y. Bekshaev and M. S. Soskin, "Transverse energy flows in vectorial fields of paraxial beams with singularities," *Opt. Commun.*, vol. 271, no. 2, pp. 332–348, 2007.
[21] J. F. Nye, "Polarization effects in the diffraction of electromagnetic waves: The role of disclinations," *Proc. Roy. Soc. A*, vol. 387, no. 1792, pp. 105–132, 1983.
[22] J. F. Nye and J. V. Hajnal, "The wave structure of monochromatic electromagnetic radiation," *Proc. Roy. Soc. A*, vol. 409, no. 1836, pp. 21–36, 1987.
[23] M. V. Berry and M. R. Dennis, "Polarization singularities in isotropic random vector waves," *Proc. Roy. Soc. A*, vol. 457, no. 2005, pp. 141–155, 2001.

[24] M. V. Berry, "Index formulae for singular lines of polarization," *J. Opt. A*, vol. 6, no. 6, pp. 675–678, 2004.
[25] C. J. R. Sheppard, "Jones and stokes parameters for polarization in three dimensions," *Phys. Rev. A*, vol. 90, no. 90, 2014, Art. no. 023809.
[26] C. J. R. Sheppard, M. Castello, and A. Diaspro, "Three-dimensional polarization algebra," *J. Opt. Soc. Amer. A*, vol. 33, no. 10, pp. 1938–1947, 2016.
[27] G. Indebetouw, "Optical vortices and their propagation," *J. Modern. Opt*, vol. 40, pp. 73–87, 1993.
[28] X. Zhao, J. Zhang, X. Pang, and G. Wan, "Properties of a strongly focused Gaussian beam with an off-axis vortex," *Opt. Commun.*, vol. 389, pp. 275–282, 2017.
[29] B. Richards and E. Wolf, "Electromagnetic diffraction in optical systems, II. Structure of the image field in aplanatic systems," *Proc. Roy. Soc. A*, vol. 253, pp. 358–379, 1959.
[30] M. Born and E. Wolf, *Principles of Optics: Electromagnetic Theory of Propagation, Interference and Diffraction of Light*, 7th (expanded) ed. Cambridge, U.K.: Cambridge Univ. Press, 1999.
[31] J. Zhang, X. Pang, and J. Ding, "Wavefront spacing and gouy phase in strongly focused fields: The role of polarization," *J. Opt. Soc. Amer. A*, vol. 34, no. 7, pp. 1132–1138, 2017.
[32] X. Pang, T. D. Visser, and E. Wolf, "Phase anomaly and phase singularities of the field in the focal region of high-numerical aperture systems," *Opt. Commun.*, vol. 284, pp. 5517–5522, 2011.